ACS OMEGA

http://pubs.acs.org/journal/acsodf

Article

Catalytic Effect of Alkali Metals on the Gasification Dissolution Reaction and Deep Reaction Behavior of Metallurgical Cokes

Xiaowei Fu, Zhijun He,* and Junhong Zhang

Cite This: *ACS Omega* 2022, 7, 38979−38989

Read Online

ACCESS | Metrics & More | Article Recommendations

ABSTRACT: In this paper, the deep reaction behaviors of tamping and top-charging cokes with different K_2CO_3 and Na_2CO_3 contents were investigated and the evolution of the functional group structure and the carbon structure of coke with the extension of the deep reaction was clarified. The results showed that the deep reaction gasification of coke steadily increased with the K_2CO_3 and Na_2CO_3 content. However, the catalytic effect of different contents of K_2CO_3 seemed to be stronger than that of different contents of Na_2CO_3. Meanwhile, the catalytic effect of alkali metals on the gasification reaction of tamping coke was more significant. The gasification dissolution of coke gradually decreased from the outside to the inside of the particle with the extension of the deep reaction, while the catalytic effect of K_2CO_3 and Na_2CO_3 seemed to be more dramatic on surface of the coke particle. In contrast, the gasification dissolution reaction on the surface of tamping coke was more severe; consequently, the surface pore area of tamping coke was much higher than that of top-charging coke. According to the variations in the functional group structure of cokes, aromatic hydrocarbon gradually became the dominant functional group in the coke structure with the extension of the deep reaction. The above variation led to a gradual decrease in the reactivity of coke, though the decomposition reactions of oxygen-containing functional groups in coke were promoted to some extent by the addition of K_2CO_3. With the extension of the deep reaction of coke, amorphous carbon was gradually transformed into sequential carbon.

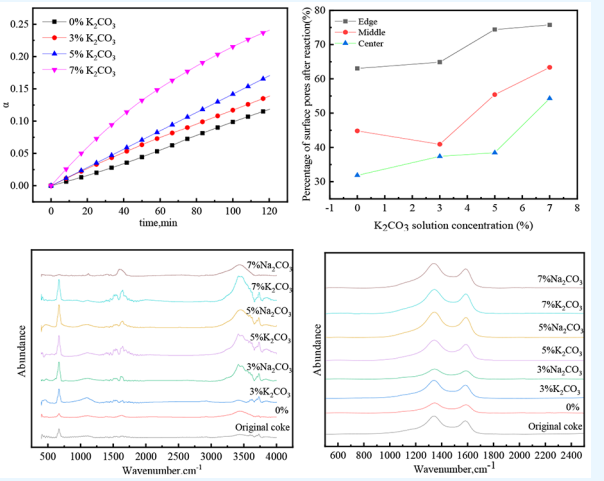

1. INTRODUCTION

Although the blast furnace process is confronting the problems of high fuel consumption and greenhouse gas emissions, the blast furnace process will remain the dominant ironmaking method for a long time. The price of metallurgical coke has gradually increased over the past few decades due to the complexity of the coking process and the resource condition of coking coal; consequently, it is essential to reduce the consumption and improve the metallurgical properties of coke.[1−5] The quality of coke directly determines the anterograde, output, coke ratio, and blast furnace fuel ratio of the blast furnace and other vital indicators, which directly affect the economic benefits of steel enterprises. As a new technology, tamping coke can reduce the reliance of ironmaking process on high-quality coking coal, since the cost of coke has been constantly increased in the past decades. Based on the cost of molten iron and the demand for sustainable development, the large-scale use of tamping coke in blast furnaces instead of conventional top-charging coke has become a trend for blast furnace ironmaking.[6−8] However, due to differences between the production process for tamping coke and that for top-charging coke, the degradation behavior of these two types of coke in the blast furnace is quite different.[9,10]

Alkali metals exist in different parts of the blast furnace in various forms during blast furnace smelting. Alkali metals mainly exist in the form of oxides, carbonates, silicates, aluminosilicates, cyanide, and interlayer compounds (e.g., C8K, C60K, etc.).[11−15] In order to further clarify the influence of alkali compounds on the gasification dissolution reaction and the deep reaction of cokes in a CO_2 atmosphere, several studies were carried out in recent years.[16,17] Wang et al.[18,19] studied the catalytic effect of alkali metals on the coke gasification reaction by studying the adsorption of alkali solution vapor on pores of coke, and the results showed that the addition of alkali compound promoted the gasification reaction and consequently the degradation of

Received: July 26, 2022
Accepted: October 5, 2022
Published: October 18, 2022

coke. Gornostaye et al.[20] and Zhou et al.[21] studied the effect of alkali compounds on the coking behavior of coking coals, and the results showed that presence of excess alkali compounds influenced the formation of the coke colloid layer, which might greatly weaken the physical and chemical properties of metallurgical coke. The mechanical strength and thermal strength of coke was significantly reduced as the amount of K and Na increased. Liu et al.[22] used the sodium leaching method to test the reactivity and postreaction strength of coke with different added alkali compounds to clarify their effect on coke gasification performance at different temperatures. The results indicated that the reactivity of coke gradually increased and the strength of coke gradually deteriorated with as the alkali compound content increased after gasification under different temperatures. Zhao et al.[23] and Yu et al.[24] found that both K and Na vapors might promote the gasification and dissolution reaction of coke; however, the catalytic effect of K on the gasification and dissolution reaction of coke was stronger than that of Na.

The above investigations showed that alkali compounds might deteriorate the quality of coke, but few studies have been conducted on the variability of the radial dissolving loss of coke particles during alkali-rich coke gasification reactions. The catalytic effect of alkali metals on the deep reaction of coke and the corresponding influence on cracks and pores of coke particles has not been sufficiently investigated, and differences in the microstructures of the gasification dissolution reaction of top-charging coke and tamping coke under different alkali metal concentrations have yet to be thoroughly investigated. In this paper, the influence of addition quantities of K_2CO_3 and Na_2CO_3 on the deep reaction of different cokes and the variation in the functional group structure and carbon structure of coke with the extension of the gasification dissolution reaction were analyzed. Meanwhile, the difference in the structure and relative density of different depths of top-charging coke and tamping coke particles during gasification dissolution process were compared.

2. EXPERIMENTAL SECTION

2.1. Materials and Preparation. Three tamping cokes (A, B, and C) and three top-charging cokes (X, Y, and Z) were selected as the samples for this study, the proximate analysis and CRI and CSR indexes of which are listed in Table 1. The proximate analysis results of tamping and top-charging cokes were quite close. In comparison, the CRI values of tamping cokes seemed to be higher than those of top-charging coke; consequently, the CSR values of top-charging cokes were higher than those of tamping cokes.

Table 1. Proximate Analysis and CRI and CSR Indexes of Coke Samples (%)[a]

sample	FC_d	V_d	A_d	CRI	CSR
A	86.45	1.85	11.71	26.72	62.02
B	86.32	1.78	11.91	26.55	63.38
C	86.26	1.82	11.92	24.68	65.39
X	85.13	1.87	13.00	21.10	68.87
Y	87.37	1.32	11.32	17.13	71.20
Z	85.84	1.20	12.97	13.03	77.52

[a]Note: FC_d refers to fixed carbon. A_d and V_d are the ash and volatile coke contents, respectively. CRI and CSR denote the coke reactivity and the coke strength after the reaction, respectively.

2.2. Gasification Dissolution Reaction of Coke. *2.2.1. K and Na Enrichment on Coke.* In order to study the influence of K and Na on the gasification reaction and the deep reaction of different types of cokes, tamping coke C and top-charging coke X with similar thermal properties were selected for comparison; this additionally prevented the influence of the gasification performance of the coke itself on the alkali metal catalysis results. Both cokes were polished into cylindrical samples with a diameter of 25 mm and height of 25 mm, and the samples were subsequently dried at 115 °C for 8 h to eliminate the influence of moisture. The prepared columnar coke samples were soaked in K_2CO_3 or Na_2CO_3 solutions with various concentrations (3%, 5%, and 7%)[25] for 24 h, then these K-enriched or Na-enriched coke samples were dried at a constant temperature of 115 °C for 12 h. The region division of a cylindrical coke sample is shown in Figure 1.

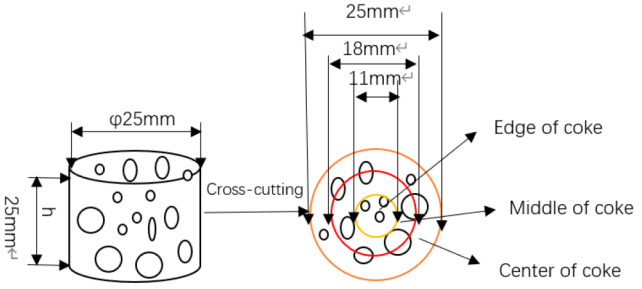

Figure 1. Deep-reaction coke sample and region division.

2.2.2. Deep Reaction of Cokes. K- or Na-enriched coke samples were loaded into a corundum crucible. The crucible was subsequently suspended under an electronic balance and heated to 1100 °C at a constant heating rate of 5 °C/min in a N_2 atmosphere with a flow rate of 2 L/min. When the coke samples reached the target temperature, N_2 was changed to CO_2 with constant flow rate of 5 L/min. After a 2 h gasification dissolution reaction, CO_2 was switched back to N_2 with a constant flow rate of 5 L/min until the coke samples cooled to ambient temperature. The real-time weight data of coke samples were recorded by a computer connected to the electronic balance. The configuration of the deep reaction device is illustrated in Figure 2.

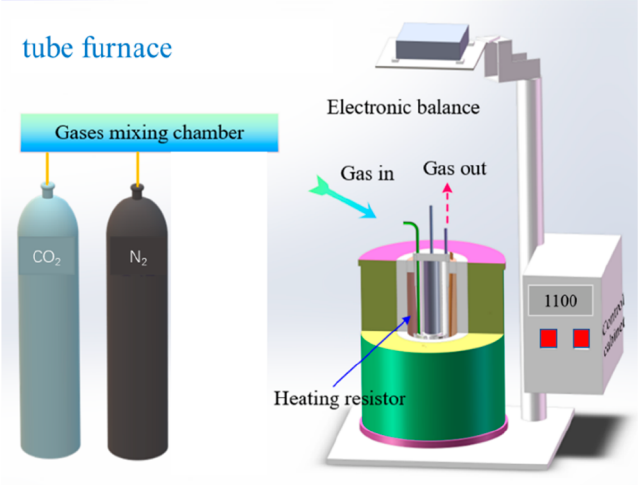

Figure 2. Configuration of the deep reaction device.

https://doi.org/10.1021/acsomega.2c04716
ACS Omega 2022, 7, 38979−38989

2.3. FTIR Measurement. Infrared spectroscopy was used to clarify variation in the functional group structure of the coke with the extension of the gasification dissolution reaction. Coke samples were crushed and dried at a constant temperature of 105 ± 5 °C for 8 h to eliminate the influence of moisture. The dried coke samples were mixed with KBr in a ratio of 1:100, then the samples were ground for 10 min to mix them thoroughly. An Agilent Technologies Cary 630 FTIR infrared spectrum analyzer was used to perform infrared spectroscopy detection on a thin slice of sample at ambient temperature. The infrared scanning range was 450−4000 cm^{-1}, and the scanning resolution was 2 cm^{-1}. Before the each test, a background scan without sample was acquired.

2.4. Determination of Functional Group Structure Parameters. The peak positions and areas of characteristic peaks were obtained by the deconvolution integral peak fitting to calculate the functional group structural parameters of coke sample, including the apparent aromaticity f_a, the aromaticity parameter I, the degree of condensation DOC, and othe xygen-containing functional group parameter "C".

Aromaticity is the ratio of aromatic carbon atoms to the total number of carbon atoms in a structural unit in a coke sample. The aromaticity value can be determined as follows:[26−30]

$$H_{al} = \frac{A_{al}}{a_{al}} = \frac{A_{2800-3000}}{a_{al}} \quad (1)$$

$$H_{ar} = \frac{A_{ar}}{a_{ar}} = \frac{A_{900-730}}{a_{ar}} \quad (2)$$

In the above formula, H_{al} and H_{ar} respectively represent the content of hydrogen in aliphatic hydrocarbons and aromatic hydrocarbons, $A_{2800-3000}$ is the peak area in the wavenumber range between 2800 and 3000 cm^{-1}, $A_{700-900}$ is the integrated area of peak to 700−900 cm^{-1}, and a_{al} and a_{ar} are fixed values (a_{al} = 746 and a_{ar} = 686).

$$\frac{H_{al}}{H} = \frac{H_{al}}{H_{al} + H_{ar}} = \frac{A_{2800-3000}}{A_{2800-3000} + A_{700-900}} \quad (3)$$

$$\frac{C_{al}}{C} = \left(\frac{H_{al}}{H} \times \frac{H}{C}\right) \Big/ \left(\frac{H_{al}}{C_{al}}\right) \quad (4)$$

$$f_a = 1 - \frac{C_{al}}{C} \quad (5)$$

Here H_{al}/H is the ratio of aliphatic (H_{al}) hydrogen atoms to total hydrogen atoms (H); C_{al}/C is the ratio of aliphatic carbon to total carbon; H/C is the ratio of aliphatic hydrogen to aliphatic carbon atoms as determined by the ultimate analysis; H_{al}/C_{al}, with a fixed value of 1.8, is the ratio of hydrogen to carbon in aliphatic group; and $A_{2800-3000}$ is the integrated area in the wavenumber range of 2800−3000 cm^{-1}, which is used to estimate the total aliphatic content (CH_3, CH_2, and CH).

Parameter I refers to the relative abundance of aromatic and aliphatic structures and can also characterize the length of the aliphatic chains. The value of I can be calculated using the following formula:

$$I = \frac{A_{700-900}}{A_{2800-3000}} \quad (6)$$

DOC represents the repetition rate of the aromatic structures and can be used to estimate the activity of aromatic structures. The DOC value can be determined using the following equation:

$$DOC = \frac{A_{700-900}}{A_{1600}} \quad (7)$$

where A_{1600} is the area of absorption peak located at the wavenumber of 1600 cm^{-1}.

$A(CH_2)/A(CH_3)$ indicates the length of the fat chain and the branching degree of fat side chains, where higher values indicate the presence of longer fat chains in the sample. $A(CH_2)/A(CH_3)$ can be determined by the following equation:

$$\frac{A(CH_2)}{A(CH_3)} = \frac{A_{2915-2940}}{A_{2950-2975}} \quad (8)$$

where $A_{2915-2940}$ and $A_{2950-2975}$ are the areas of peaks located in wavenumber ranges of 2915−2940 cm^{-1} and 2950−2975 cm^{-1}, respectively.

"C" indicates the maturity of the coke and represents the ratio of C═O to C═C, the value of which can be calculated as follows:

$$"C" = \frac{A_{1650-1800}}{A_{1650-1800} + A_{1600}} \quad (9)$$

where $A_{1650-1800}$ is the area of the peak located between 1650 and 1800 cm^{-1}.

2.5. Raman Spectroscopy Inspection. A high spectral resolution Raman spectrometer (LabRAM HR Evolution) was used to analyze the carbon structure characteristics of coke samples. The coke samples were tested in the wavenumber range of 100−2500 cm^{-1} at an ambient temperature of 20−25 °C with a wavelength of 532 nm.[31−33] The resolution of the test results was better than 0.65 cm^{-1}.

2.6. Calculation of Fixed and Nonfixed Carbon. The parameters of I_{D1}/I_G, I_{D3}/I_G, I_G/I_{all}, and L_a represent the degree of graphite-like structure in the graphite layer, the amorphous carbon fraction, the content of the graphite-like crystal structure, and the size of crystallite, respectively.[34,35] L_a can be calculated as follows:[36,37]

$$L_a = C(\lambda)(I_{D1}/I_G)^{-1} \quad (10)$$

$$C(\lambda) = C_0 + \lambda C_1 \quad (11)$$

where $C(\lambda)$ is the correction factor for the wavelength, C_0 is −12.6 nm, C_1 is 0.033 nm, and the effective wavelength range is 400−700 nm. The wavelength used in the paper is 532 nm.

3. RESULTS AND DISCUSSION

3.1. K_2CO_3 and Na_2CO_3 Absorption of Coke Samples. The adsorption capacity of K_2CO_3 and Na_2CO_3 in coke samples is shown in Figure 3.

As shown in Figure 3, the adsorption capacity of cokes increased with the concentration of the soaking solution, while the adsorption capacity of K_2CO_3 was slightly higher than that of Na_2CO_3. As shown in Table 2, the adsorption capacity of sample X for the K_2CO_3 solution was slightly larger than that for the Na_2CO_3 solution when the concentration was 3% but the gasification catalysis of Na_2CO_3 was smaller than that of K_2CO_3, which indicates that the difference in the gasification reaction was not due to the concentration. The difference may be caused by the different coke structures.

3.2. Experimental Results and Analysis. The gasification dissolution reaction curves of C and X coke samples with various amounts of added K_2CO_3 or Na_2CO_3 are respectively shown in Figures 4 and 5. The effect of different alkali metal contents on

https://doi.org/10.1021/acsomega.2c04716
ACS Omega 2022, 7, 38979−38989

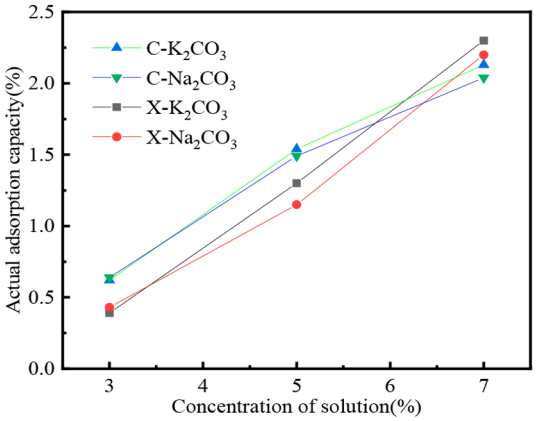

Figure 3. K_2CO_3 and Na_2CO_3 adsorption capacity of coke samples (%).

Table 2. Effect of Alkali Metal Addition on the Gasification Degree of Cokes (%)

sample	K_2CO_3 concentration	degree of vaporization	Na_2CO_3 concentration	degree of vaporization
C	0%	11.93	0%	11.93
	3%	13.89	3%	13.60
	5%	17.12	5%	15.49
	7%	24.08	7%	20.15
X	0%	10.98	0%	10.98
	3%	13.29	3%	14.47
	5%	15.84	5%	15.04
	7%	20.80	7%	15.95

the coke gasification dissolution is shown in Table 2. It can be seen from above data that the catalytic effect of K_2CO_3 on C coke seemed to be much stronger than that on X coke during the gasification dissolution reaction, while the catalytic effect on both coke samples was stronger with higher amounts of added K_2CO_3.

The catalytic effect of Na_2CO_3 on C and X coke samples was very close at low Na_2CO_3 addition conditions, but the gasification dissolution reaction of C coke was significantly stronger when concentration of the Na_2CO_3 solution was higher than 5%. Besides, for the deep reaction of coke, the catalytic effect of Na_2CO_3 on coke seemed to be slightly weaker than that of K_2CO_3, and the difference in the catalytic effect increased with the solution concentration.

3.3. Influence of the Alkali Metal Microstructure on the Coke Structure. *3.3.1. Microscopic Morphology of Coke.* The structure of coke is a critical factor for the gasification of coke, which is of great importance for evaluating coke quality. Hence, the radical differences of coke samples at different stages of the gasification dissolution reaction were observed by SEM, and the proportion of the pore area at different radical positions was analyzed to clarify the variation in the pore structure of coke with the extension of the deep reaction. The variations of the microstructure at different radical positions of coke after the gasification dissolution reaction for different K_2CO_3 addition conditions are shown in Figures 6−9. The depth range of 0−7 mm from the surface of the coke particle is defined as the edge, the depth range of 8−14 mm from the surface of the coke particle is defined as the middle, and the depth range of 15−25 mm from the surface of the coke particle is defined as the center.

As can be seen, the dissolution of pore structures for both C and X coke samples gradually developed at the centers of the coke particles with the extension of the deep reaction, while the number of pores on the surface of the coke particle gradually decreased. Due to the limitation of CO_2 diffusion, the gasification reaction on the surface of the coke particle was more violent. Consequently, the dissolution on the surface structure was found to be more severe; the superficial pore structure seemed to be loose, and the surface of coke particle became rough after the gasification test. In addition, the dissolution degree of C coke was more severe compared to that of X coke. The pore walls at the edges of coke particles became thinner, and the perforation of large internal pores was also noticed. As a result, many internal pores were connected with the extension of the deep reaction, and the superficial porosity of the coke particle increased significantly. As the amount of added K_2CO_3 or Na_2CO_3 increased, the degree of carbon dissolution on the surface of the coke particle intensified significantly and the superficial damage in the microstructure became more severe. It was also observed that the dissolution degree in the middle part of coke was the relatively weaker compared to that at the surface. It is worth noting that the carbon dissolution in middle part of C coke was significantly higher than that of X coke. The dissolution degree in the middle part of coke particle increased under K_2CO_3 or Na_2CO_3 addition conditions, which led to the formation of cracks in microstructures of the cokes. These formed cracks provided an ideal channel for the diffusion of CO_2 and consequently resulted in severe dissolution in the middle part of the coke structure.

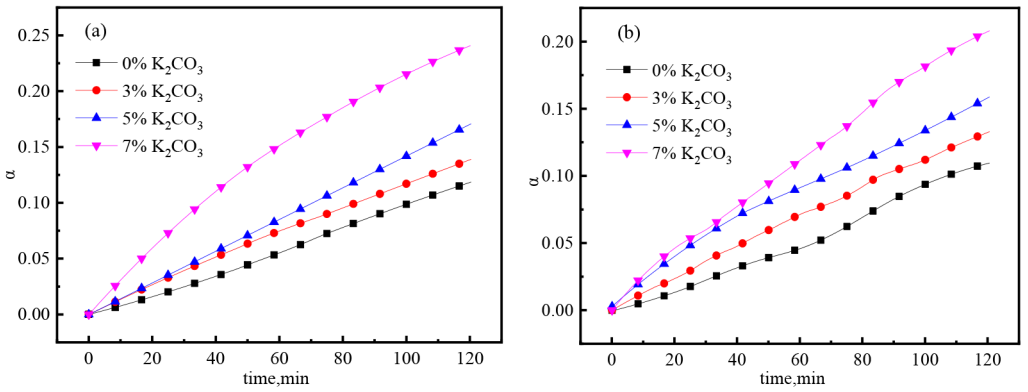

Figure 4. Effect of K_2CO_3 addition on the deep reaction of cokes (a) C and (b) X.

https://doi.org/10.1021/acsomega.2c04716
ACS Omega 2022, 7, 38979−38989

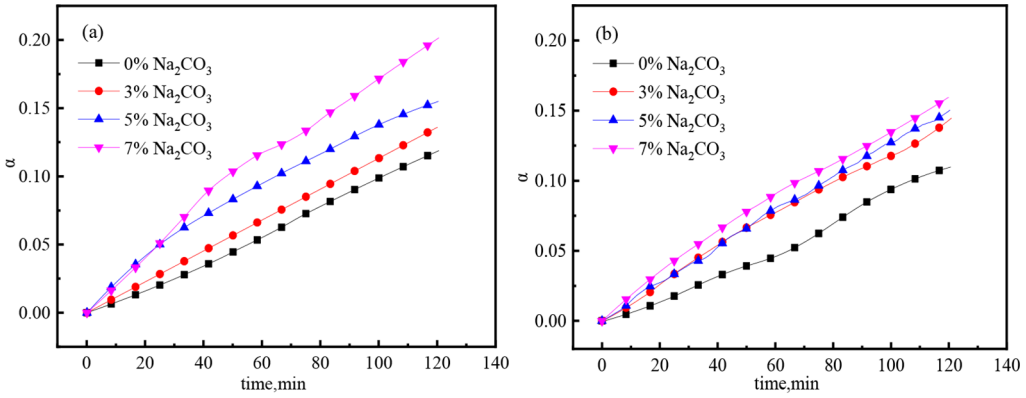

Figure 5. Effect of Na_2CO_3 addition on the deep reaction of cokes (a) C and (b) X.

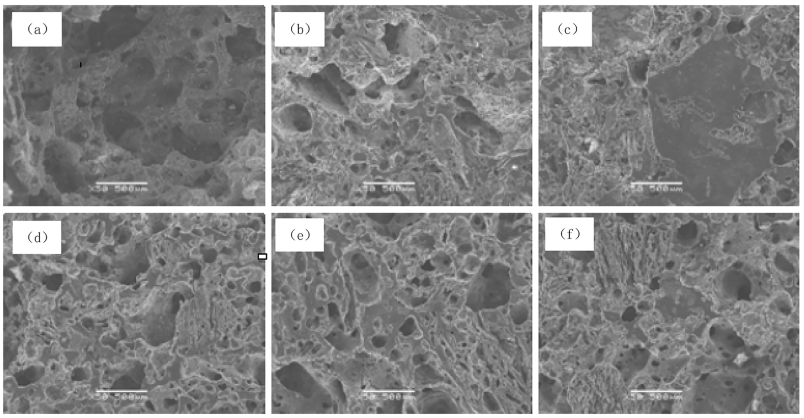

Figure 6. Microstructure of original coke after the reaction: (a) edge of X, (b) middle of X, (c) center of X, and (d) edge.

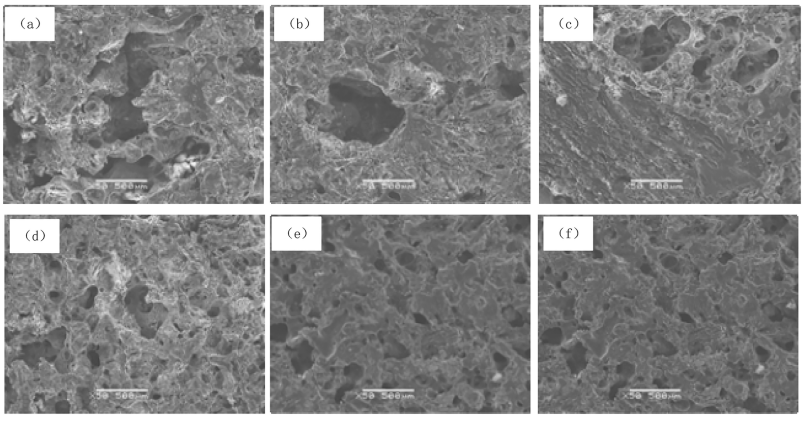

Figure 7. Microstructure of 3% K_2CO_3 coke after the reaction: (a) edge of X, (b) middle of X, (c) center of X, (d) edge of C, (e) middle of C, and (f) center of C.

Image-Pro Plus software was applied to analyze the SEM pictures of different coke samples in order to quantitatively compare the area proportions of the pores at different depths of the coke structure, and the results are shown in Figure 10. It can be seen that the proportion of the surface pore area increased with the amount of added K_2CO_3 and Na_2CO_3. The surface pore area proportion under K_2CO_3 addition conditions was slightly higher than that of under Na_2CO_3 conditions, while the proportion of the surface pore area gradually decreased as the depth increased and increased with the amount of added K_2CO_3 and Na_2CO_3. This was possibly due to the catalytic effect of the alkali metal and the diffusion of CO_2 into internal parts of the coke particles. On the basis of the above analysis results, the gasification reaction mechanism of the coke particle is summarized in Figure 11.

3.4. Functional Group Structural Evolution in Coke Samples during Gasification. The gasification experiments of coke samples were conduted under various K_2CO_3 and Na_2CO_3 addition conditions, and the functional group structures of coke samples at different stage of gasification were analyzed. The infrared spectra of different coke samples are shown in Figure 12. All spectra were smoothed and baseline-corrected using OMINIC software. The absorption peaks at different wavenumber positions are related to the relative

https://doi.org/10.1021/acsomega.2c04716
ACS Omega 2022, 7, 38979−38989

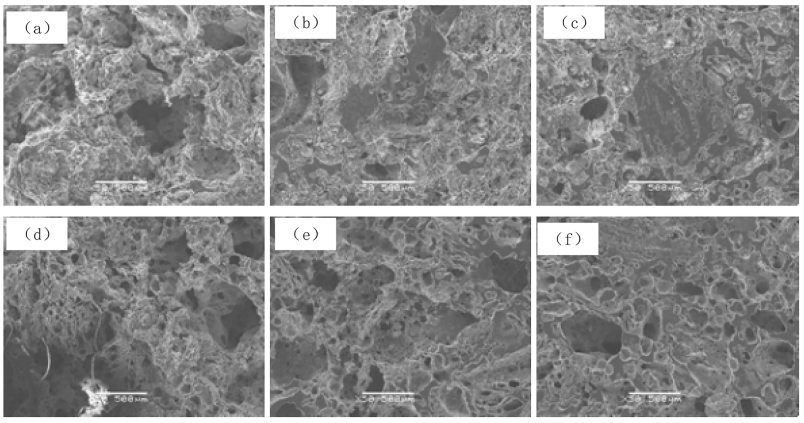

Figure 8. Microstructure of 5% K_2CO_3 coke after the reaction: (a) edge of X, (b) middle of X, (c) center of X, (d) edge of C, (e) middle of C, and (f) center of C.

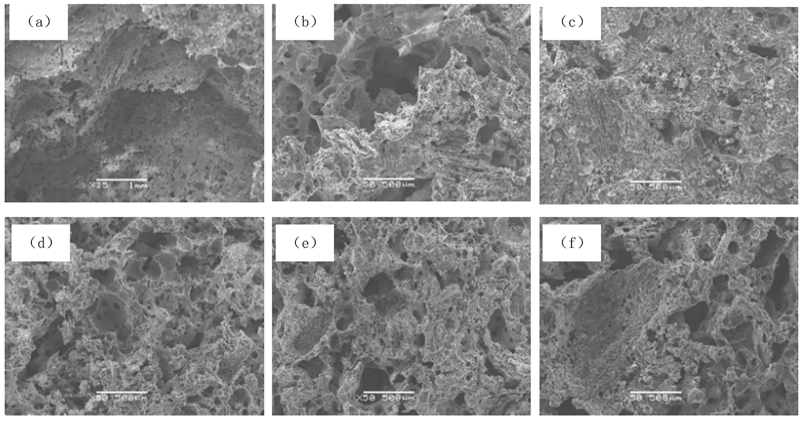

Figure 9. Microstructure of 7% K_2CO_3 coke after the reaction: (a) edge of X, (b) middle of X, (c) center of X, (d) edge of C, (e) middle of C, and (f) center of C.

amount of the corresponding functional groups in the coke sample. The original infrared spectra were deconvolutioned into several independent peaks to calculate the functional group structures of the coke samples, and the deconvolution process is illustrated in Figure 13. The infrared absorption peaks, peak areas, and other data can be obtained through this process. The affiliation relationship between absorption peaks at different wavenumber positions and functional groups is shown in Table 3.

It can be seem from Figure 12 that similarities there are similarities in the spectra of the selected samples in the wavenumber range between 3000 and 3750 cm^{-1}, indicating the abundance of −OH and $-CH_3$ functional groups in the selected coke samples. The intensities of the above-mentioned absorption peaks in the X sample were noticed to be significantly higher than those in the C sample after the gasification reaction, which indicated the high proportion of −OH and $-CH_3$ functional groups in the X sample. The absorption peak between 900 and 1040 cm^{-1} represents the ash content of the coke sample, which was noticed to be much higher in the C sample than the X sample. Meanwhile, the absorbance of coke gradually increased with the extension of the deep reaction, indicating the production of ash in coke samples with the consumption of the carbon matrix.

The functional group structural parameters of coke samples were calculated according to the data of independent peaks from deconvolution; the detailed calculation method was described previously. The functional group structural parameters results of different coke samples are listed in Table 4. It can be seen from the data that the f_a and I values both increased after the gasification dissolution reaction, which indicated that the aromatic functional groups were relatively stable during the gasification of coke. Meanwhile, the degree of condensation of the coke samples was significantly higher after the reaction index test, indicating that the aromatic hydrocarbons gradually became more stable with the extension of the gasification dissolution reaction. Under K_2CO_3 and Na_2CO_3 addition conditions, the f_a and I values both decreased as the amount of added K_2CO_3 and Na_2CO_3 increased after gasification, while the DOC value decreased as the amount of alkali metals increased. The above phenomenon implies that the both K_2CO_3 and Na_2CO_3 have an obvious catalytic effect on −OH and $-CH_3$ groups and that the catalytic intensity has a positive relationship with the amount of added K_2CO_3 and Na_2CO_3, while the effect of K_2CO_3 and Na_2CO_3 on the reaction behavior of aromatic functional groups was insignificant. The catalytic effect of K_2CO_3 and Na_2CO_3 on the C coke sample seemed to be higher than that on the X coke. The higher $A(CH_2)/A(CH_3)$ value of C suggests that the length of the carbon chain in the structure of C was longer than that in X, that is, the instability of C during the chemical reaction. As the amount of added K_2CO_3 and Na_2CO_3 increased, the collapse of the carbon chain in the C coke sample intensified significantly and the $A(CH_2)/A(CH_3)$ value of C sharply decreased. However, the $A(CH_2)/A(CH_3)$

https://doi.org/10.1021/acsomega.2c04716
ACS Omega 2022, 7, 38979−38989

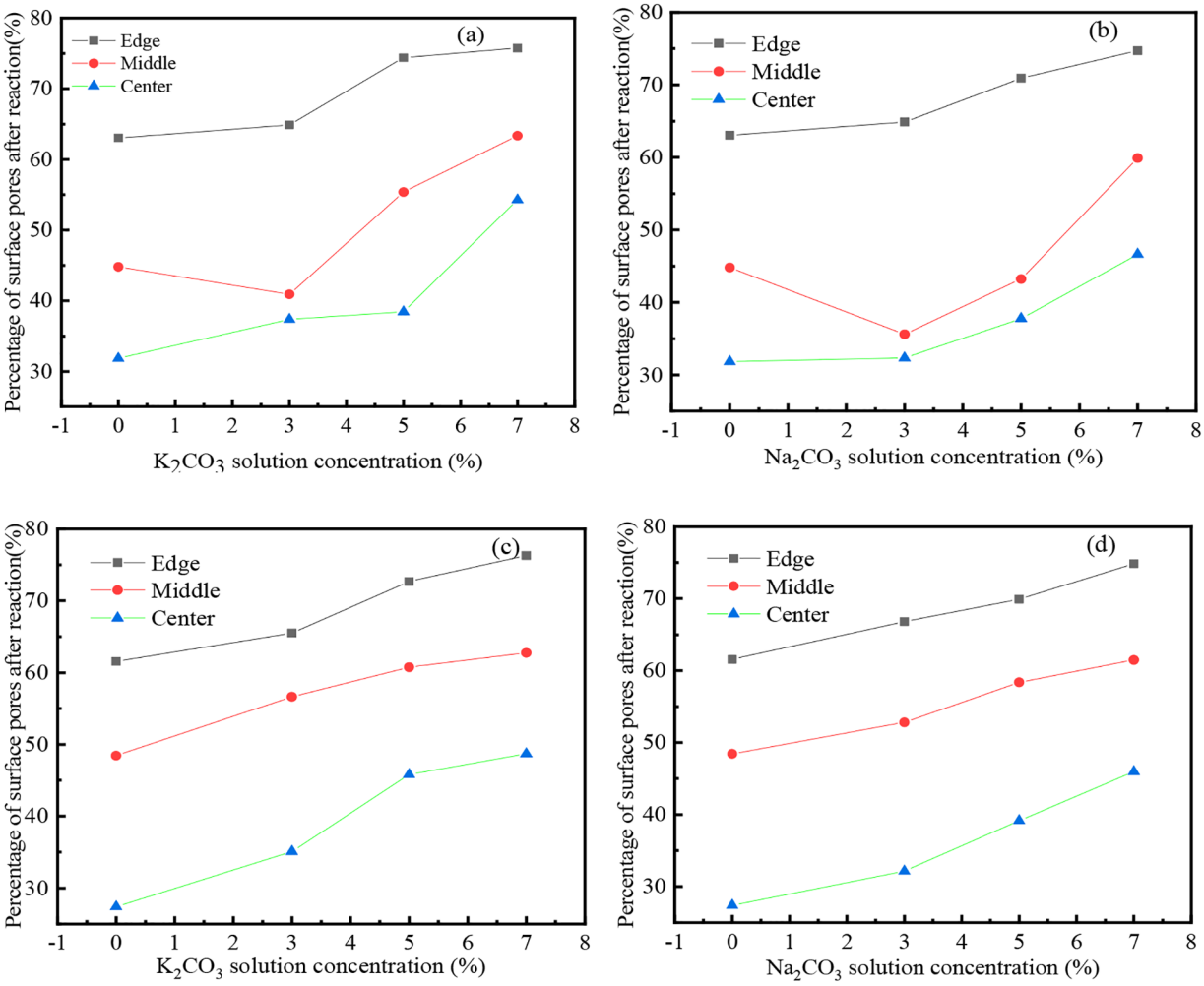

Figure 10. Surface pore area proportion (%) of coke after the reaction for (a and b) sample C and (c and d) sample X.

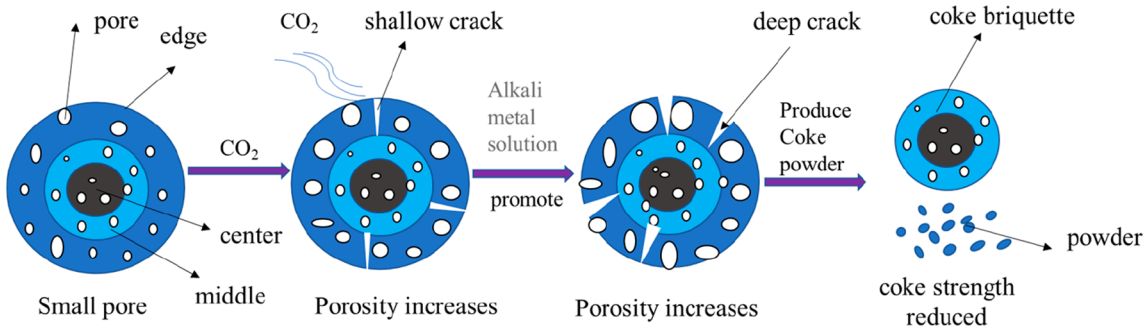

Figure 11. Schematic diagram of the pore structure of coke and the alkali metal reaction.

value of X was observed to be quite stable with different K_2CO_3 and Na_2CO_3 addition conditions. Besides, the number of oxygen-containing functional groups in both coke samples was noted to be slightly lower after the gasification dissolution reaction. The value of "*C*" sharply decreased with as the amount of added K_2CO_3 and Na_2CO_3 increased, indicating the strong catalytic effect of the alkali metal on the decomposition of oxygen-containing functional groups; additionally, the catalytic intensity increased with the alkali metal content.[38,39]

3.5. Raman Spectroscopy Analysis. The carbon structures of C and X coke samples after reaction index test under various K_2CO_3 and Na_2CO_3 addition conditions were analyzed by Raman spectroscopy, and the test results are shown in Figure 14. The deconvolution process and the affiliation of independent peaks are respectively shown in Figure 15 and Table 5. The structural parameters of coke samples were respectively calculated according to the peak areas of independent peaks, and the results are shown in Table 6.

The variation in carbon structural parameters I_{D1}/I_G, I_{D3}/I_G, I_G/I_{all}, and L_a of C and X coke samples after the gasification reaction under different K_2CO_3 and Na_2CO_3 addition conditions is shown in Table 6. The I_{D1}/I_G and I_{D3}/I_G values decreased with the extension of the deep reaction, which indicated an increase in the proportion of graphite-like carbon in

https://doi.org/10.1021/acsomega.2c04716
ACS Omega 2022, 7, 38979−38989

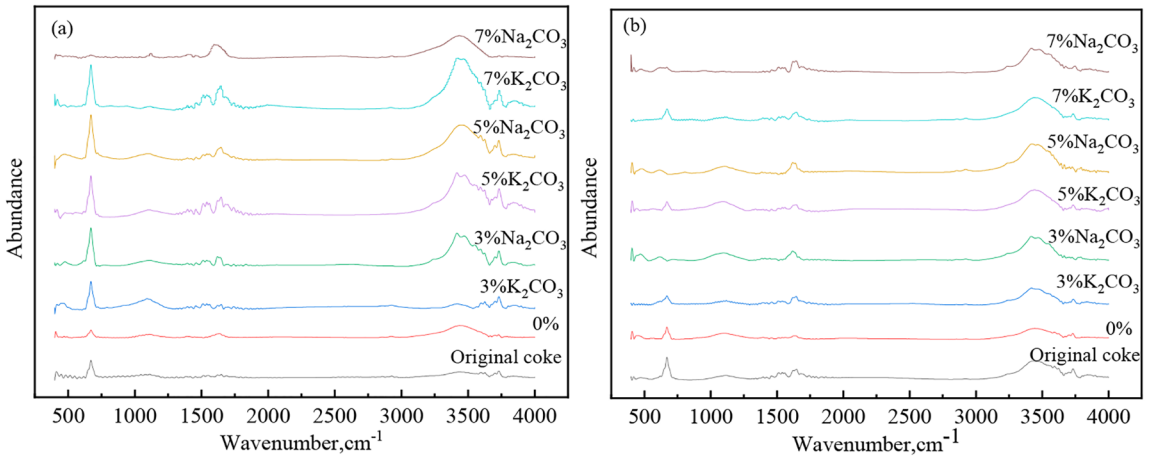

Figure 12. Infrared spectra of cokes (a) C and (b) X.

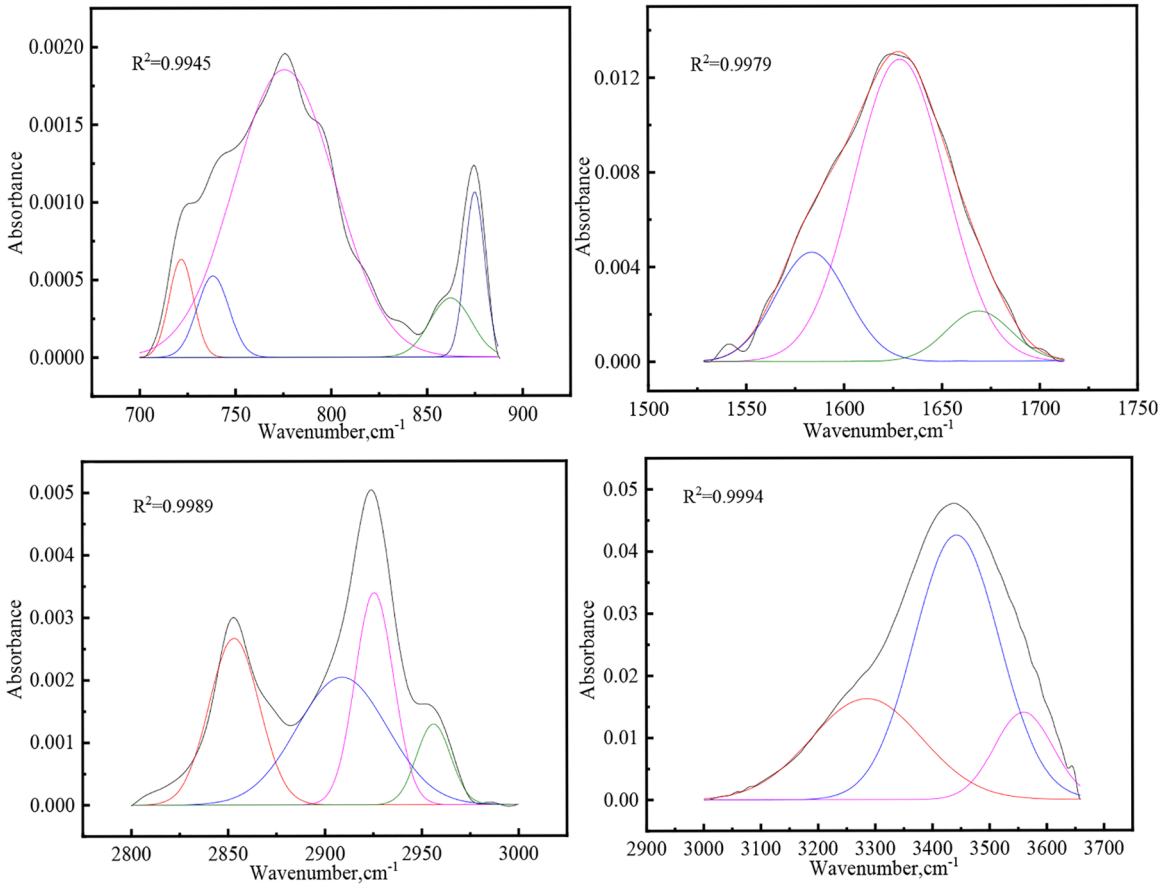

Figure 13. Peak-fitting process on the infrared spectra of coke.

the coke sample. Meanwhile, the decrease in the fraction of nongraphitic crystalline carbon indicated that the irregular carbon in coke was transformed into graphite-like carbon over the course of the gasification reaction; the increase of the I_G/I_{all} value also proved that both the proportion of the graphite-like crystal structure and the grain size increased during gasification.

According to the changes in carbon structural parameters, the existence of both K and Na led to a reduction in graphitization, grain size, and the graphite-like crystal structure content and an increase in fraction of amorphous carbon in coke samples. The above phenomena indicate that the addition of K and Na might facilitate the gasification dissolution reaction process of coke, as it inhibits the conversion of amorphous carbon to ordered carbon during gasification; for example, most active sites had amorphous carbon structures during gasification. Meanwhile, the addition of K and Na would promote the decomposition of stable aromatic rings into small hydrocarbons, consequently preventing the graphitization of coke during the gasification reaction. Besides, the catalytic effect of K was noticed to be stronger than that of Na, especial for the condition of tamping coke in comparison to top-charging coke. The fraction of amorphous carbon was higher due to the lower degree of

https://doi.org/10.1021/acsomega.2c04716
ACS Omega 2022, 7, 38979−38989

Table 3. Correspondence of Functional Groups

peaks	wavenumber (cm^{-1})	functional groups
1	3550−3200	−OH
	3030	−CH (aromatic ring)
2	2950 (shoulders)	$-CH_3$
3	2920, 2860	$-CH_3$ cycloalkanes or aliphatic hydrocarbons
4	2858−2847	$-CH_2$
5	2780−2350	−COOH
6	1610	carbonyl-substituted aromatic hydrocarbons
	1590−1470	aromatic hydrocarbon
	1460	$-CH_2$, $-CH_3$, inorganic carbonate
7	1375	$-CH_3$
8	1330−1110	C−O (phenols, alcohol ethers, and lipids)
	1040−900	ash
9	860	CH (1,2,4-, 2,4,5-, and 1,2,3,4,5-substituted aromatic hydrocarbons)
	750	CH (1,2-substituted aromatic hydrocarbons)
	700	CH (single-substituted or 1,3-substituted aromatic hydrocarbons)
10	475	−SH

Table 4. Functional Group Structural Parameters of Cokes

sample	f_a	I	DOC	$A(CH_2)/A(CH_3)$	"C"
original C	0.9989	0.5259	1.5145	4.9631	0.2933
C−0%	0.9990	0.5006	4.1211	4.9576	0.2589
C−3% K_2CO_3	0.9988	0.4337	1.5671	4.7871	0.1983
C−3% Na_2CO_3	0.9988	0.4044	2.2209	4.8019	0.2587
C−5% K_2CO_3	0.9986	0.3128	1.6393	4.3148	0.1156
C−5% Na_2CO_3	0.9986	0.3321	2.3025	4.4012	0.2586
C−7% K_2CO_3	0.9985	0.1450	1.6929	4.0610	0.0903
C−7% Na_2CO_3	0.9985	0.1246	2.6361	4.0901	0.2585
original X	0.9974	0.2182	1.5094	3.2780	0.5498
X−0%	0.9974	0.2043	4.2305	3.1795	0.4871
X−3% K_2CO_3	0.9973	0.1433	2.1158	3.1543	0.3459
X−3% Na_2CO_3	0.9973	0.1631	2.0833	3.1607	0.3927
X−5% K_2CO_3	0.9972	0.1036	2.2013	3.1233	0.2325
X−5% Na_2CO_3	0.9972	0.1425	2.1129	3.1421	0.3348
X−7% K_2CO_3	0.9971	0.0798	3.3059	3.0991	0.1257
X−7% Na_2CO_3	0.9972	0.1239	3.1708	3.2009	0.2242

graphitization in tamping coke, which was possibly the reason for the stronger catalytic effect. A higher resistance of top-charging coke to the alkali metal was noticed; hence, the metallurgical property of top-charging coke in a blast furnace is thought to be superior.

CONCLUSIONS

In this paper, the gasification dissolution reaction and the deep reaction between coke with different K_2CO_3 and Na_2CO_3 contents and CO_2 were studied and the variation of the pore microstructure, functional group structure, and carbon structure with the extension of gasification and dissolution reaction and the deep reaction were analyzed. The results can be summarized as follows:

(1) As the K_2CO_3 and Na_2CO_3 content in the coke sample increased, the gasification degree in the deep reactions of both tamping coke and top-charging coke gradually increased. No significant difference was noticed in the catalytic effect of K_2CO_3 and Na_2CO_3 when the concentration of soaking solution was increased from 3% to 5%. However, the catalytic effect of K_2CO_3 was seemed to be much stronger than that of Na_2CO_3 when the concentration of the applied solution was 7%.

(2) With the extension of gasification dissolution, the difference in the gasification dissolution extent between the exterior and interior of the coke samples became more significant. The catalytic effect of K_2CO_3 and Na_2CO_3 seemed to be stronger on the exterior of the coke particle.

(3) Due to the stability of the aromatic structure, the proportion of aromatic hydrocarbons in coke gradually increased with the extension of the gasification dissolution reaction. The addition of K_2CO_3 may significantly

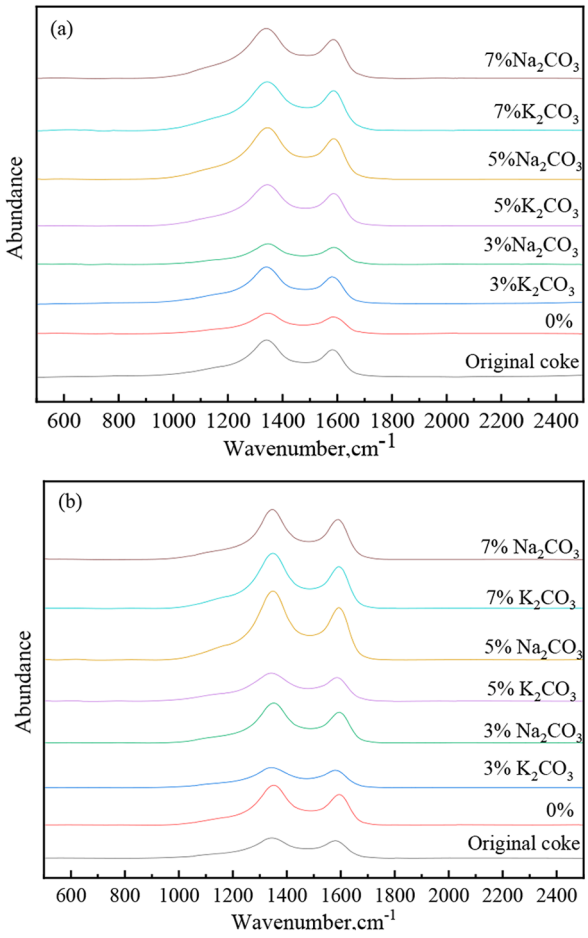

Figure 14. Raman spectra of cokes (a) C and (b) X.

Table 5. Correspondence between the Raman Peak and the Carbon Structure

peak	peak position (cm^{-1})	carbon structure
G	1600	ideal graphite lattice
D_1	1350	chaotic graphite lattice (incomplete carbon crystallites (chaotic atoms))
D_2	1620	disordered graphite lattice (irregular arrangement of carbon crystallites)
D_3	1500	amorphous carbon
D_4	1200	disordered graphite lattice (polyene-like structure)

https://doi.org/10.1021/acsomega.2c04716
ACS Omega 2022, 7, 38979−38989

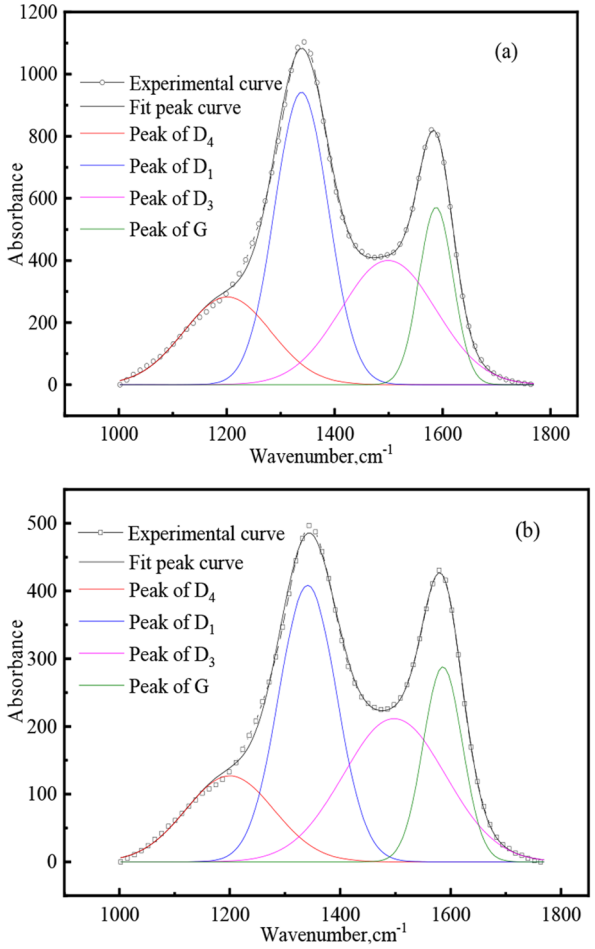

Figure 15. Peak-fitting process on Raman spectra of cokes (a) C and (b) X.

Table 6. Carbon structure parameters of coke

sample	I_{D1}/I_G	I_{D3}/I_G	I_G/I_{all}	L_a
original C	2.60	1.96	0.15	5.08
C−0%	2.08	1.87	0.16	5.06
C−3% K_2CO_3	2.58	2.08	0.15	5.04
C−3% Na_2CO_3	2.45	1.90	0.15	4.78
C−5% K_2CO_3	2.55	2.13	0.14	4.98
C−5% Na_2CO_3	2.33	1.94	0.14	4.54
C−7% K_2CO_3	2.53	2.36	0.13	4.94
C−7% Na_2CO_3	2.19	1.96	0.14	4.29
original X	2.09	1.91	0.17	4.08
X−0%	1.98	0.65	0.23	3.87
X−3% K_2CO_3	2.08	1.01	0.23	4.07
X−3% Na_2CO_3	2.05	1.03	0.20	4.01
X−5% K_2CO_3	2.07	1.39	0.22	4.05
X−5% Na_2CO_3	2.03	1.40	0.18	3.98
X−7% K_2CO_3	2.07	1.71	0.22	4.04

catalyze the decomposition of oxygen-containing functional groups in the coke, and the catalytic effect seems to increase with the concentration of the soaking solution.

(4) The gasification dissolution reaction of coke could be catalyzed by the addition of K_2CO_3 and Na_2CO_3, as the presence of the alkali metal might inhibit the conversion of amorphous carbon to ordered carbon during gasification. The catalytic effect of K_2CO_3 and Na_2CO_3 on the gasification dissolution reaction of tamping coke seemed to be stronger than that of top-charging coke, which was possibly due to the lower degree of graphitization and the higher fraction of amorphous carbon in tamping cokes.

AUTHOR INFORMATION

Corresponding Author

Zhijun He − *School of Materials and Metallurgy, University of Science and Technology Liaoning, Anshan, Liaoning 114051, P. R. China*; Phone: +8613998001790; Email: hzhj2002@126.com

Authors

Xiaowei Fu − *School of Materials and Metallurgy, University of Science and Technology Liaoning, Anshan, Liaoning 114051, P. R. China*; orcid.org/0000-0001-9718-750X

Junhong Zhang − *School of Materials and Metallurgy, University of Science and Technology Liaoning, Anshan, Liaoning 114051, P. R. China*

Complete contact information is available at: https://pubs.acs.org/10.1021/acsomega.2c04716

Notes

The authors declare no competing financial interest.

ACKNOWLEDGMENTS

This work was financially supported by the National Natural Science Foundation of China (51874171) and the Xingliao Talent Plan (XLYC2002064).

REFERENCES

(1) Li, K.; Zhang, J.; Zhang, Y.; Liu, Z.; Jiang, X. Analysis on development of iron-making process based on the principle of energy-saving and emission reduction. *Chin. J. Proc. Eng.* **2014**, *14* (1), 162−172.

(2) Vega, M. F.; Díaz-Faes, E.; Barriocanal, C. Influence of the heating rate on the quality of metallurgical coke. *ACS omega* **2021**, *6*, 34615−34623.

(3) Zhang, L.; Wang, G.; Xue, Q.; Zuo, H.; She, X.; Wang, J. Effect of preheating on coking coal and metallurgical coke properties: A review. *Fuel. Process. Technol.* **2021**, *221*, 106942.

(4) Gao, C.-k.; Na, H.-m.; Song, K.; Tian, F.; Strawa, N.; Du, T. Technologies-based potential analysis on saving energy and water of China's iron and steel industry. *Sci. Total Environ.* **2020**, *699*, 134225.

(5) Suresh, A.; Panda, A.; Dominic, M.; Chandaliya, V. K.; Guha, M.; Singh, R.; Dash, P. S. Utilisation of low-grade raw materials for preparation of reactive catalysed-coke for blast furnace application. *Ironmaking Steelmaking* **2019**, *46*, 491−497.

(6) Xing, X.; Zhang, G.; Rogers, H.; Zulli, P.; Ostrovski, O. Effects of annealing on microstructure and microstrength of metallurgical coke. *Metall. Mater. Trans. B* **2014**, *45*, 106−112.

(7) Wei, Q.; Pang, K.; Wu, J.; Liang, C. Coke characteristics and formation mechanism based on the hot tamping coking. *Journal of Analytical and Applied Pyrolysis* **2022**, *161*, 105381.

(8) Tiwari, H.; Shisani, V.; Sahu, B.; Sabat, K.; Mittal, D. Influence of the prime hard coking coal in stamp charge cokemaking: true or false. *Metall. Res. Technol.* **2020**, *117*, 412.

(9) Rejdak, M.; Strugała, A.; Sobolewski, A. Stamp-charged coke-making technology-The effect of charge density and the addition of semi-soft coals on the structural, textural and quality parameters of coke. *Energies* **2021**, *14* (12), 3401.

(10) Xu, R.; Dai, B.; Wang, W.; Schenk, J.; Bhattacharyya, A.; Xue, Z. Gasification reactivity and structure evolution of metallurgical coke under H_2O/CO_2 atmosphere. *Energy Fuel.* **2018**, *32*, 1188−1195.

(11) Matjie, R.; Bunt, J.; Stokes, W.; Bijzet, H.; Mphahlele, K.; Uwaoma, R.; Strydom, C. Interactions between kaolinite, organic matter, and potassium compounds at elevated temperatures during pyrolysis of caking coal and its density-separated fractions. *Energy Fuel.* **2021**, *35*, 13268−13280.
(12) Nechaeva, T.; Fedorova, N.; Ismagilov, Z. Influence of activation on the pore structure of adsorbents obtained from coal-alkali mixtures. *Coke Chem.* **2017**, *60*, 239−242.
(13) Gornostayev, S.; Tanskanen, P.; Heikkinen, E.-P.; Kerkkonen, O.; Härkki, J. An example of alkalization of SiO_2 in a blast furnace coke. *Energy Fuel.* **2007**, *21*, 2637−2641.
(14) Kurunov, I.; Titov, V.; Emel'yanov, V.; Lysenko, S.; Arzamastsev, A. Analysis of the behavior of alkalis in a blast furnace. *Metallurgist* **2009**, *53*, 533−542.
(15) Li, K.; Zhang, J.; Barati, M.; Khanna, R.; Liu, Z.; Zhong, J.; Ning, X.; Ren, S.; Yang, T.; Sahajwalla, V. Influence of alkaline (Na, K) vapors on carbon and mineral behavior in blast furnace cokes. *Fuel* **2015**, *145*, 202−213.
(16) Chang, Z. Y.; Wang, P.; Zhang, J. L.; Jiao, K. X.; Zhang, Y. Q.; Liu, Z. J. Effect of CO_2 and H_2O on gasification dissolution and deep reaction of coke. *International Journal of Minerals, Metallurgy, and Materials* **2018**, *25*, 1402−1411.
(17) Rejdak, M.; Wasielewski, R. Mechanical compaction of coking coals for carbonization in stamp-charging coke oven batteries. *Physicochem. Probl. Miner. Process.* **2015**, *51*, 151−161.
(18) Wang, M.; Wei, G.; Yang, S.; Zhu, R.; Yang, L. Effect of alkali (K/Na) metal vapor on the metallurgical properties of coke in CO_2-O_2-N_2 mixed atmosphere. *Energy* **2022**, *257*, 124748.
(19) Wang, H.; Zhang, J.; Zhong, J. Effect of potassium vapor on deterioration of top-charging and tamping coke. *China Metall.* **2018**, *2018* (28), 12−14.
(20) Gornostayev, S.; Kerkkonen, O.; Harkki, J. Behaviour of coal associated minerals during coking and blast furnace processes - A review. *Steel Res. Int.* **2009**, *80* (6), 390−395.
(21) Zhou, Y.; Wang, G.; Tian, Y.; Luo, D.; An, L.; Wang, X.; Jin, W. Effect of K and Na on Technological Properties of Coking Coal and Performances of Tamping Coke. *Coal Conversion* **2016**, *39* (3), 72−76.
(22) Liu, Y.; Zhang, B.; Wang, F.; Liang, L. The influence of alkaline metal on thermal properties of coke. *Coal Conversion* **2008**, *31* (3), 43−46.
(23) Zhao, H.-b.; Cheng, S.-s. New cognition on coke degradation by potassium and sodium in alkali enriched regions and quantificational control model for BF. *J. Univ. Sci. Technol. Beijing* **2012**, *34*, 333−341.
(24) Yu, D.; Guo, R.; Liang, Y.; Liu, L.; Chen, P. Effects of alkali metal on solution loss and coke degradation. *Metall. Res. Technol.* **2019**, *116*, 609.
(25) Wang, G.; Ren, S.; Zhang, J.; Ning, X.; Liang, W.; Zhang, N.; Wang, C. Influence mechanism of alkali metals on CO_2 gasification properties of metallurgical coke. *Chem. Eng. J.* **2020**, *387*, 124093.
(26) Chen, Y.; Mastalerz, M.; Schimmelmann, A. Characterization of chemical functional groups in macerals across different coal ranks via micro-FTIR spectroscopy. *Int. J. Coal Geol.* **2012**, *104*, 22−33.
(27) He, X.; Liu, X.; Nie, B.; Song, D. FTIR and Raman spectroscopy characterization of functional groups in various rank coals. *Fuel* **2017**, *206*, 555−563.
(28) Keliang, P.; Wenguo, X.; Changsui, Z. Investigation on pyrolysis characteristic of natural coke using thermogravimetric and Fourier-transform infrared method. *Journal of analytical and applied pyrolysis* **2007**, *80*, 77−84.
(29) Wang, Y.; Pang, Q. H.; He, Z. J.; Liu, J. H.; Zhang, J. H.; Zhan, W. L. Kinetic analysis on non-isothermal combustion of several urban biomass fuels. *BioRes.* **2019**, *14* (4), 7702−7718.
(30) Jiang, J.; Yang, W.; Cheng, Y.; Liu, Z.; Zhang, Q.; Zhao, K. Molecular structure characterization of middle-high rank coal via XRD, Raman and FTIR spectroscopy: Implications for coalification. *Fuel* **2019**, *239*, 559−572.
(31) Rantitsch, G.; Bhattacharyya, A.; Schenk, J.; Lünsdorf, N. K. Assessing the quality of metallurgical coke by Raman spectroscopy. *Int. J. Coal Geol.* **2014**, *130*, 1−7.
(32) Rantitsch, G.; Bhattacharyya, A.; Günbati, A.; Schulten, M. A.; Schenk, J.; Letofsky-Papst, I.; Albering, J. Microstructural evolution of metallurgical coke: Evidence from Raman spectroscopy. *Int. J. Coal Geol.* **2020**, *227*, 103546.
(33) Rantitsch, G.; Bhattacharyya, A.; Schenk, J. Microstructural evolution of blast furnace coke during experimental heating—The IFORS approach. *BHM Berg-und Hüttenmännische Monatshefte* **2019**, *164*, 257−260.
(34) Guizani, C.; Jeguirim, M.; Gadiou, R.; Escudero Sanz, F. J.; Salvador, S. Biomass char gasification by H_2O, CO_2 and their mixture: Evolution of chemical, textural and structural properties of the chars. *Energy* **2016**, *112*, 133−145.
(35) Gong, X.; Guo, Z.; Wang, Z. Effects of Fe_2O_3 on pyrolysis reactivity of demineralized higher rank coal and its char structure. *CIESC. J.* **2009**, *60* (9), 2321−2325.
(36) Bai, B.; Guo, Q.; Li, Y.; Hu, X.; Ma, J. Catalytic gasification of crushed coke and changes of structural characteristics. *Energy Fuels* **2018**, *32*, 3356−3367.
(37) Zickler, G. A.; Smarsly, B.; Gierlinger, N.; Peterlik, H.; Paris, O. A reconsideration of the relationship between the crystallite size L_a of carbons determined by X-ray diffraction and Raman spectroscopy. *Carbon* **2006**, *44*, 3239−3246.
(38) Long, F. J.; Sykes, K. W. The catalysis of the carbon monoxide-steam reaction. *Proc. R. Soc. Lond. A* **1952**, *215* (1120), 111−119.
(39) Wigmans, T.; Hoogland, A.; Tromp, P.; Moulijn, J. A. The influence of potassium carbonate on surface area development and reactivity during gasification of activated carbon by carbon dioxide. *Carbon* **1983**, *21*, 13−22.

https://doi.org/10.1021/acsomega.2c04716
ACS Omega 2022, 7, 38979−38989